Title: Thermal analysis of polylactic acid under high CO_2 pressure applied in supercritical impregnation and foaming process design

Authors: Robert Kuska, Stoja Milovanovic, Sulamith Frerich, Jasna Ivanovic

PII: S0896-8446(18)30498-4
DOI: https://doi.org/10.1016/j.supflu.2018.10.008
Reference: SUPFLU 4385

To appear in: *J. of Supercritical Fluids*

Received date: 27-7-2018
Revised date: 10-10-2018
Accepted date: 10-10-2018

Please cite this article as: Kuska R, Milovanovic S, Frerich S, Ivanovic J, Thermal analysis of polylactic acid under high CO_2 pressure applied in supercritical impregnation and foaming process design, *The Journal of Supercritical Fluids* (2018), https://doi.org/10.1016/j.supflu.2018.10.008

Thermal analysis of polylactic acid under high CO_2 pressure applied in supercritical impregnation and foaming process design

Robert Kuska[a], Stoja Milovanovic[b], Sulamith Frerich[a]*, Jasna Ivanovic[b]*

[a]*Institute of Thermo and Fluid Dynamics, Ruhr-University Bochum, Universitätsstraße 150, 44801 Bochum, Germany*

[b]*University of Belgrade, Faculty of Technology and Metallurgy, Department of Organic Chemical Technology, Karnegijeva 4, 11000 Belgrade, Republic of Serbia*

***Corresponding Authors:**

E-Mail: frerich@vvp.rub.de; Tel: +49 2343226496 (S. Frerich)

E-Mail: jasnai@tmf.bg.ac.rs; Tel: +38 1113303795 (J. Ivanovic)

Graphical abstract

Abbreviations

PLA-E	Extrusion grade PLA
PLA-I	Injection grade PLA
SFE	Supercritical fluid extraction
SSI	Supercritical solvent impregnation
s-F	Static (foaming) process without circulation (without antibacterial agents)
s-SSI	Static process without circulation
d-SSI	Dynamic process with circulation
SFE-SSI	Coupled process of SFE and SSI operated in semi-continuous mode

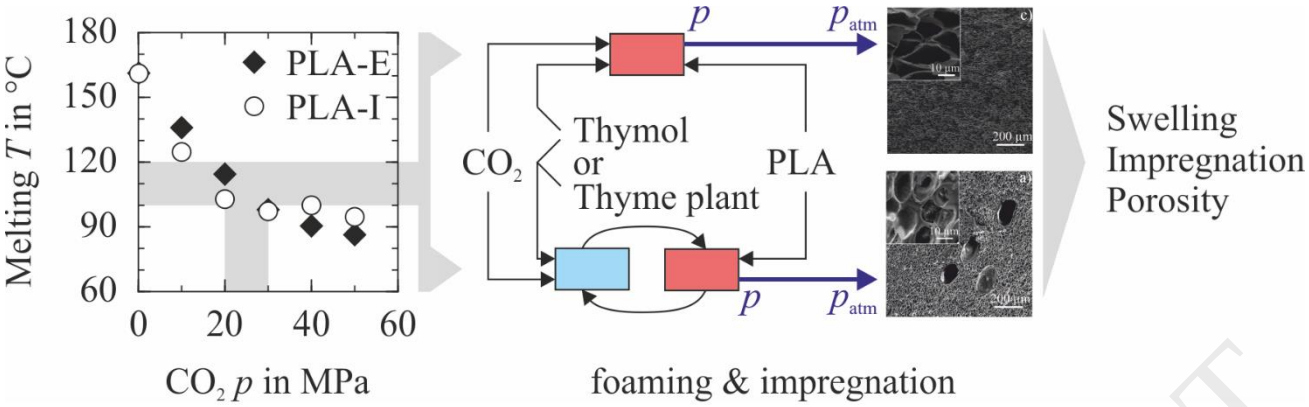

Highlights

- PLA melting and crystallinity were studied by HP-DSC at CO_2 pressure of 10-50 MPa.
- The lowest melting point and crystallinity degree of PLA are observed at 20-30 MPa.
- Batch and semi-continuous processes for PLA impregnation with foaming were studied.
- DSC and HP-DSC showed greater effect of CO_2 pressure on crystallinity then foaming.
- Pore size of the neat and thymol/thyme extract containing PLA foams was 15-200 μm.

Abstract

Thermal properties of extrusion and injection grade polylactic acid (PLA) were analysed using high pressure differential scanning calorimetry (HP-DSC) under CO_2 pressures of up to 50 MPa. The greatest depression of melting point and degree of crystallinity of the samples occurred at 20-30 MPa (~97-115 °C). Batch and semi-continuous processes for supercritical foaming and impregnation of PLA with thymol or thyme extract were performed at 30 MPa and 100-110 °C to prevent thymol degradation, decrease heating requirements and ease polymer processing. At these conditions, PLA foams containing 5.6% or 1.1% of thymol and 0.7% of thyme extract were obtained using static or dynamic batch impregnation and semi-continuous extraction-impregnation process for 7 h, respectively. DSC and HP-DSC analyses revealed more pronounced effect of $scCO_2$ plasticizing than foaming on PLA crystallinity. Neat and impregnated PLA foams with pores size of 15-200 μm have potential for food packaging, biomedical and insulation applications.

Keywords: High-pressure DSC; Polylactic acid; Supercritical impregnation; Supercritical foaming; Thymol; Thyme extract

Introduction

The great interest in polylactic acid (PLA) for the production of biodegradable cellular materials for drug delivery, medical (scaffolding) and packaging applications (cushioning, insulation) is due to its sustainable production and reasonably good mechanical, optical and barrier properties [1–4]. An inherently slow crystallization and poor foaming ability of semi-crystalline PLA limits its use for high-performance applications [5]. Exposing PLA to dense CO_2 under isothermal and non-isothermal conditions can alter melt-strength and crystallization kinetics of the polymer and improve its foaming ability [6–12]. Already at pressures below 5 MPa, dense CO_2 present in the polymer matrix acts like a molecular lubricant [9–11]. It enhances the chain mobility by weakening intermolecular and

intramolecular interactions [13] and reduces the melting (T_m) and crystallization temperature (T_s) as well as the melt viscosity [7,11]. Consequently, this affects the formed types, distribution, size and stability of crystals [6]. $ScCO_2$ plasticizing is advantageous for the low temperatures processing of the heat and shear sensitive polymers and additives with less energy consumption [14,15]. Furthermore, a rapid depressurization of the system of PLA and dense CO_2 induces supersaturation in the metastable melt phase, which results in the nucleation of CO_2 bubbles [16,17]. The bubble nucleation, growth and connectivity are dependent on the viscosity and crystallinity of the polymer/gas solution. They are controlled by the operating conditions and the material shaping and cooling profile [14,16,18]. Whereas foaming with CO_2 has been commonly carried out with amorphous polymers (i.e. polystyrene as one of the most frequently studied), foaming of semi-crystalline polymers is more challenging due to very narrow foam-processing window which is result of their insufficient melt strength at high temperatures and crystallization at low temperatures [17]. To achieve foaming of semi-crystalline polymers within the processing window, a reasonable solubility of the blowing agent in polymer phase, high enough melt strength and availability of setting mechanisms (crystallization or vitrification) are required. In this regard, plasticizing effect of the CO_2 used as a blowing agent is significant [19–21].

High pressure differential scanning calorimetry (HP-DSC) enables *in situ* monitoring of thermal transitions of polymers and determination of thermal properties in presence of compressed fluids [15,22,23]. Available up-to-date reports on HP-DSC analysis of PLA are limited to the measurements at low to moderately high CO_2 pressures (1 - 18 MPa) [22,24–26]. Huang et al. [22] reported the decreasing effect in T_m of PLA is levelled off in the pressure range of 15-18 MPa [22]. This could be due to a dominating hydrostatic effect, which decreases free volume in the polymer matrix and chain mobility, and change the melting behaviour of the polymer [22,27–29]. Therefore, the study of thermal transitions at even higher pressures would extend the up-to-date knowledge on

melting and crystallization behaviour of semi-crystalline PLA with providing new valuable information for a high-pressure process design.

An outbreak and fast spreading of drug-resistant bacterial strains that cause fatal infections in humans and animals urged research on alternative and natural antibacterial agents and their incorporation into polymer materials used in biomedicine and food industry [30–36]. Thyme extracts and their most abundant component thymol have been proven for strong antibacterial activity against Gram-positive and Gram-negative bacterial strains [33,37,38] including methicillin resistant staphylococci [39]. Supercritical CO_2 ($scCO_2$) is a good solvent for thymol [15,40] and due to its high diffusivity into different polymer matrices it can be efficiently used for polymer loading with thymol [15,30,32,36,41].

Sorption of $scCO_2$ induces polymer swelling, which promotes incorporation and transport of loaded substances within a polymer matrix [42–45]. Polymers can be impregnated using $scCO_2$ in a batch or semi-continuous process [15,31,46,47]. As for impregnations with plant extracts, the use of a coupled supercritical fluid extraction (SFE) and supercritical solvent impregnation (SSI) process is recommended [30,31,46]. It minimizes extract loss, processing time and energy consumption [31]. SSI allows the control of the amount and penetration depth of an impregnating substance as well as the resulting foam morphology by adjustments of pressure, temperature, depressurization rate and contact time [31]. In SSI processes $scCO_2$ can be used as a “green” solvent, foaming agent and impregnation medium within one processing step [30,31].

This study was aimed to investigate melting and crystallization temperatures of PLA within an extended CO_2 pressure range (up to 50 MPa) as well as separate and coupled effects of sorbed $scCO_2$ and supercritical foaming on degree of crystallinity at various pressures using HP-DSC. The results of thermal analysis were applied for design of the batch and semi-continuous processes for production of PLA foams impregnated with natural antibacterial agents (thymol and thyme extract).

The results were used to explain the foam morphology and investigate alternative routes for further process optimizations.

1. Material and Methods

1.1. Materials

Samples of commercial extrusion (PLA-E, Ingeo™ Biopolymer 2003D, $M_w \approx 210000$ g/mol) and injection grade (PLA-I, Ingeo™ Biopolymer 3052D, $M_w \approx 160000$ g/mol) polylactic acid were obtained from NatureWorks LLC (Blair, Nebraska, USA). The transparent beads of PLA-E and PLA-I with a density of 1237.0 kg/m³ are mixtures of poly(L-lactic acid) and poly(D-lactic acid) containing 4.25 ± 0.55 and 4.15 ± 0.45% D-isomer, respectively. Carbon dioxide (purity of 99.9%) was supplied by Messer-Technogas (Serbia) and Yara International (Germany). Indium (purity of 99.999%, $T_m = 156.6$ °C, $\Delta H_m = 28.45$ J/g) was purchased from Alfa Aesar GmbH & Co. KG (Karlsruhe, Germany). Thymol (purity > 99%, Sigma Aldrich, Germany) and the aerial part of cultivated thyme (*Thymus vulgaris* L) (donated by manufacturer BIOSS-Petrović Slobodan i ostali, Beograd, Serbia) were used for impregnation processes.

1.2. High pressure differential scanning calorimetry

A differential scanning calorimeter (C80, Setaram, France) in combination with an ultra-high pressure gas panel were used to study thermal properties of neat PLA and PLA foams under high CO_2 pressure. It is used in three different methods aimed to study:

1. Melting and crystallization temperatures, T_m and T_s, at 0.1 - 50 MPa,

2. Separate and coupled effects of sorbed CO_2 and supercritical foaming within HP-DSC apparatus at various pressures, and

3. Crystallinity of samples already foamed in high pressure view cell at pressures 10 - 30 MPa.

All methods also carried out the degree of crystallinity (χ_c).

For the first method, measurements at atmospheric and elevated pressure (10 - 50 MPa) were performed with crucibles with a volume of 12.3 mL and 3 mL, respectively. All samples were heated from 30 °C to 200 °C at a rate of 0.1 °C/min to eliminate previous thermal and stress histories, and kept at a constant temperature of 200 °C for 1 h. Afterwards, they were cooled down to 30 °C at the rate of 0.1 °C/min (**Figs. 1a** and **1b**). Subsequently, these steps were repeated for the actual determination of T_m, T_s and degree of crystallinity (χ_c) (**Figs. 1e** and **1f**, procedure of calculation is reported in supplementary materials **Fig. S1**). The heating rate has been chosen according to recommendation of the manufacturer (0.001 to 2 °C/min) and experience with HP-DSC measurements using other polymers [30,31] to reduce potential noises and thermal lag in the system. The melting enthalpy (ΔH_m) was calculated using the Calisto Data Acquisition software (Version 1.38) by linear baseline integration. The overall crystallinity of the PLA samples was determined using **Eq. 1** [48]:

$$\chi_c = \frac{\Delta H_m - \Delta H_{cc}}{\Delta H_m^0} \cdot 100\ \%. \qquad (1)$$

ΔH_m is the experimental melting enthalpy, ΔH_{cc} is the experimental cold crystallization enthalpy and ΔH_m^0 is a theoretical enthalpy for 100% crystalline PLA with a value of 93.6 J/g [49]. Indium was used for the calibration of the temperatures and ΔH_m at ambient and high pressures.

Figure 1

The second method is a simulated foaming process within the HP-DSC. For that purpose, the PLA samples, dried at 80 °C in vacuum, were placed in the DSC. The cells were pressurized to 10, 20 or 30 MPa and then heated to 100, 120 or 140 °C, respectively, as in the batch foaming process (**Fig. 1c**). After reaching the process conditions, CO_2 is released at a rate of about 0.8 MPa/s to foam the sample. At atmospheric pressure, the system is cooled down to 30 °C. In one case, the pressure is increased again to the foaming pressure to monitor thermal behaviour at an elevated pressure

(**Fig. 1e**), while in the second case the pressure remains at atmospheric pressure (**Fig. 1f**). In both cases, the temperature is increased to 180 °C.

Finally, for the third method, the HP-DSC at atmospheric pressure was used to test PLA samples after batch-foaming to study their thermal properties (**Figs. 1d** and **1f**).

1.3. Impregnation

Three types of supercritical solvent impregnation of PLA samples were investigated:

- s-SSI: Static process without circulation of the supercritical solution to load PLA with thymol,
- d-SSI: Dynamic process with circulation of the supercritical solution to load PLA with thymol, and
- SFE-SSI: Coupled process of SFE and SSI operated in semi-continuous mode to load PLA with thyme extract.

The s-SSI process was performed in a high pressure view cell (25 mL) equipped with a CCD camera described elsewhere [40] at CO_2 pressures of 20 - 30 MPa and corresponding melting temperatures of the PLA samples (100 - 120 °C) for 2 and 24 h. The PLA beads were melted at 180 °C for 10 min in cylindrical glass recipients ($d \approx 10$ mm, $h \approx 15$ mm) in order to monitor swelling at the same time as the foaming process. For comparative analysis, also static foaming of PLA (s-F) without impregnation was performed in the same apparatus at the same operating conditions. The swelling extent (S) is calculated by comparing the rising PLA melt level (h) with the initial level (h_0), which are equivalent to the change in volume (volume after time V_t and initial volume V_0) because the radius of the glass recipient is constant. The change in height of the melt surface is measured by the ImageJ Software:

$$S = \frac{V_t - V_0}{V_0} \cdot 100\ \% = \frac{h - h_0}{h_0} \cdot 100\ \% \qquad (2)$$

The mass ratio of PLA (0.24 ± 0.01 g) and thymol was 1:1 at the beginning of the impregnation process. The decompression rate at the end of the process was 3 MPa/s.

The d-SSI and SFE-SSI processes were performed in a laboratory scale unit (HPEA 500, Eurotechnica, Germany) presented in **Fig. 2**. It enables operations in batch, semi-continuous or continuous mode and consists of separate extraction (V = 280 mL, T_{max} = 121 °C) and impregnation vessels (V = 100 mL, T_{max} = 250 °C). The PLA samples (0.24 ± 0.01 g) within a cylindrical Teflon mould (d_{in} = 8.25 mm, d_{out} = 10.35 mm, h = 20 mm) with perforated wall and bottom were placed in the impregnation vessel (Adsorber).

In case of d-SSI process, thymol (1.8 g) in a glass recipient, covered with a wire mesh, was placed in the extractor vessel. Spherical glass beads (d = 6.8 ± 01 mm) were placed under and above the glass recipient to provide an evenly distributed flow through the vessel. The mean mass ratio of thymol and PLA (m_T / m_{PLA}) was 7.6 ± 0.4 to achieve a similar saturation of $scCO_2$ with thymol as in s-SSI.

In case of SFE-SSI process, thyme plant material (m_{Thyme} = 25 g) was placed in the extractor inside a basket filling the whole cross section of the vessel to force $scCO_2$ to flow through the plant material. The mass ratio of thyme and PLA (m_{Thyme} / m_{PLA}) was 102.3 ± 3.0.

For both, d-SSI and SFE-SSI, the operating pressure of 30 MPa was applied. The extractor was then heated to 40 °C and the adsorber to 110 °C. The 10 °C increase compared to the s-SSI process was to compensate heat losses along pipes and gear pump in the HPEA unit. While d-SSI is performed in a single pressurizing step, SFE-SSI uses a semi-continuous mode. After achieving the operating conditions in both vessels, 2 h of circulation of the supercritical solution followed. After the circulation was stopped, only the adsorber was depressurized and then refilled and repressurized with fresh CO_2. The circulation continued for additional 2 or 5 h. The mean decompression rates were 3.8 ± 1.0 MPa/s.

Both processes (d-SSI and SFE-SSI) were categorized by the time of impregnation without (static, t_{st}) and with circulation (dynamic, t_{dyn}) of the supercritical solution, gear pump frequency and the achieved loading.

Figure 2

The loading of thymol and thyme extract (L) is calculated using **Eq. 3**:

$$L = \frac{m_L}{m_L + m_{PLA}} \cdot 100\ \% \qquad (3)$$

m_L is the mass of loaded substance and m_{PLA} the initial mass of PLA. The value of m_L is calculated as the difference between masses of the impregnated PLA sample and m_{PLA} weighted using an analytical balance (accuracy±0.01 mg).

1.4. Analysis of PLA foams' morphology

The morphology of the neat and impregnated PLA samples was investigated by the field emission scanning electron microscopy (FE-SEM) using a Mira3 XMU TESCAN a.s. (Brno, Czech Republic) with an accelerating voltage of 10 kV. The foams were first immersed in liquid nitrogen for about 5 min and fractured. Thereafter, the samples were coated with a thin layer of Au/Pd (85/15) using a sputter coater (POLARON SC502, Fisons Instruments, Ipswich) prior to FE-SEM.

The foam porosity ε is calculated by **Eq. 4**:

$$\varepsilon = \left(1 - \frac{\rho_f}{\rho_0}\right) \cdot 100\ \%, \qquad (4)$$

where ρ_0 is the density of the PLA beads with a value of 1237.0 kg/m^3, ρ_f is the density of the foam determined using a specific gravity bottle (pycnometer) with a volume of 25 mL by the water displacement method in accordance to ASTM D792-0022:

$$\rho_f = \frac{\rho_{H2O} \cdot w_1}{w_1 + w_2 - w_3} \quad (5)$$

The density of water is $\rho_{H2O} = 997.9$ kg/m³ at 21.6 °C, w_1 is the mass of the foamed sample, w_2 is the mass of the pycnometer filled with water and w_3 is the mass of the pycnometer containing both water and sample.

All the measurement results within the study are expressed as mean values from triplicate measurements with standard deviation.

2. Results and discussion

To design a high pressure process, the knowledge of the melting and crystallization behaviour of the polymer exposed to a supercritical fluid is essential. It allows a better understanding of the phenomena and an identification of the operating pressure and temperature conditions. For that purpose, a research strategy, outlined by the following three steps, was used in the present study:

1. Identification of melting and crystallization temperature ranges of PLA at pressures between 0.1 and 50 MPa using a HP-DSC (see method 1, section 1.2)
2. Design of batch and semi-continuous processes for supercritical impregnation and foaming of PLA at pressures and temperatures identified for PLA melting. It is followed by the optimization of impregnation time and operating regimes to maximize the thymol or thyme extract loading and foam morphology.
3. Analysis of the influences of adsorbed CO_2 pressure and PLA foaming on degree of crystallinity (methods 2 and 3, section 1.2) at the optimal operating conditions identified in the previous steps (2 and 3).

2.1. Thermal properties of PLA at various CO_2 pressures

The initial step was to obtain HP-DSC heating and cooling curves to determine melting and crystallization temperatures as well as melting enthalpies to calculate degree of crystallinity (**Table S1**). In **Fig. 3**, the melting curves for both PLA-types at pressures of 0.1 MPa to 50 MPa are displayed. Both polymers show a characteristic double peak melting, which is best pronounced at atmospheric pressure. This is due to morphologically different crystals [50]. The first appearing peak at a lower temperature is assigned to less organized and stable crystals as previously suggested by Yokohara & Yamaguchi (1970) [51]. The second peak, when more stable crystals are liquefied, is therefore taken as indicator for T_m [52] (**Fig. S1**). Appearance of two melting peaks in melting endotherms is result of lamellar rearrangements during crystallization and, consequently, presence of various crystalline structures in PLA. α'-crystals of PLA with high L-lactic acid content (96–100 %) grow at higher temperatures (155-165 °C). Less α'-crystals are formed at 140 °C or even below 120 °C, and spontaneously transform into stable α-modification during heating [53,54].

The curve at 10 MPa demonstrates the shift of T_m with CO_2 pressurization. In the case of PLA-I (**Fig. 3b**), a greater T_m temperature depression occurs with a wider melting range of about 38 °C, whereas PLA-E (**Fig. 3a**) has a range of about 21 °C.

Figure 3

The phase transition temperatures as well as the crystallinity level of the PLA-E and PLA-I samples determined by HP-DSC at atmospheric pressure and CO_2 pressures of 10 - 50 MPa are given in **Fig. 4**. A steep T_m **(Fig. 4a**) depression is identified with increasing pressures up to 20 MPa (PLA-I) and 30 MPa (PLA-E), respectively. This T_m shift for both PLA samples indicates a plasticizing effect of CO_2 on the polymers. Further pressure increase does not reduce T_m significantly (PLA-E) or is

almost imperceptible (PLA-I). The two observed depression regions on the T_m curve (**Fig. 4a**) can be addressed to “solubility effects” and “pressure effects” [20]. “Solubility effects” occur at moderate pressures by sorption of CO_2. In this pressure regime the melting depression of PLA-E is between -2.12 and -2.55 °C/MPa and of PLA-I between -2.14 and -3.68 °C/MPa. The T_m depression is in the same range as reported for semi-crystalline poly(L-lactic acid) exposed to CO_2 by using HP-DSC at pressures of 2 MPa (from -2 to -7 °C/MPa) [24], visual method at 27.6 MPa (-2 °C/MPa) [20] or linear variable differential transformer technique at 41.4 MPa (-1.56 °C/MPa) [44]. The minimum T_m (so called "kink point") is attributed to the balanced CO_2 dissolution in the polymer phase. Any further CO_2 feed tends to shift T_m toward higher values [15,20].

Figure 4

Crystallinity level of PLA samples was affected by cooling process. After a 56% drop of crystallinity level at pressures above 20 MPa compared to atmospheric pressure, a shift of χ_c towards higher values is observed, especially in case of PLA-I. An increase in saturation pressure promotes the nucleation of crystals, while the low cooling rate (0.1 °C/min) promotes the formation of more perfect crystals [8]. Consequently, the crystals growth prevails over their nucleation. It favours formation of the more ordered structures, which results in increase of crystallization temperatures (T_s) at pressures above 20 and 30 MPa [7,8]. At 20 MPa and 30 MPa the greatest depression of melting point of the PLA samples was observed (~97 - 115 °C, **Table S1**). These pressures were chosen for PLA impregnation experiments aiming to prevent degradation of thymol (< 142 °C [55]) and decreased heating requirements

2.2. Design and optimization of impregnation processes

The s-SSI process aimed the optimization of the processing time regarding the thymol loading and foam morphology. It was performed in a view cell with pressures between 20 and 30 MPa and temperatures of 100 - 120 °C (determined by HP-DSC). For this purpose, PLA that is less plasticized by $scCO_2$ (PLA-E) was used. The results on thymol loading in PLA-E are shown in **Table 1**. The impregnation is favoured by low $scCO_2$ densities and increased process time. All achieved loading values are sufficient to ensure an antimicrobial effect of the polymer [56], even at the maximum CO_2 density of 661.9 kg/m³.

For the evaluation of the PLA-E swelling extent, the s-SSI process was performed for 2 h and 24 h with and without (s-F) thymol within the ρ_{CO2} range of 401.2 - 661.9 kg/m^3. The addition of thymol affects the swelling significantly and results in about twice as high values than with $scCO_2$ only (**Fig. 5**). Thymol acts as molecular lubricant which results in increased free volume of the polymer matrix of PLA and consequently higher gas sorption [41,46]. A prolonged exposure of PLA-E (24 h) to either $scCO_2$ only or $scCO_2$ with thymol has led to a 40 - 90% greater swelling extent in comparison to the first 2 h of exposure. The lowest swelling extents with thymol were achieved with the greatest $scCO_2$ density.

Figure 5

According to the achieved thymol loadings and swelling behaviour during the static processes (s-SSI, s-F), a pressure of 30 MPa and a temperature of 100 °C (ρ_{CO2} = 661.9 kg/m³) were chosen for the optimization of the dynamic processes performed in the HPEA unit. The d-SSI process was

optimized to maximize the thymol loading by the variation of a t_{st}, t_{dyn} and the gear pump frequency. The results are presented in **Table 2**.

First of all, the circulation time t_{dyn} of CO_2 and the gear pump frequency were varied (regimes 1 - 3). Both had no significant influence on the thymol loading, because most of thymol remained inside of the glass recipient during the experiment. One reason could be related to the CO_2 flow direction in the vessel from bottom to top, which enables a flow past the recipient without being loaded with thymol at all. For this reason, a static period (t_{st}) of 2 h was used as starting condition. Thereafter, the reduced circulation frequency was used, and the processing time was varied (regimes 4 and 5). These modifications of the process were intended to allow a higher saturation of supercritical phase with thymol and allow more time for diffusion of supercritical solution ($scCO_2$+thymol) into polymer matrix.

Accordingly, introduction of the static processing of 2 h prior to additional dynamic led to almost no remaining thymol in the glass recipient, whereby thymol loading of PLA-E was almost twice as much as without a static pre-process for the same total processing time (regime 3). An increase in t_{dyn} to 5 h (regime 5), resulted in additional 55% thymol loading increase in PLA-E. The same regimes with circulation (4 and 5) were applied for PLA-I impregnation. The PLA-I foams had 24% (regime 4) and 82% (regime 5) lower thymol loadings compared to the PLA-E foams. In contrast to PLA-E, an increase of t_{dyn} from 2 h to 5 h resulted in a decrease of about 60% of thymol loading in the PLA-I foam. This is due to a different plasticizing behaviour of the PLA samples. As demonstrated in section 2.1, the melting and crystallization temperatures of PLA-I are lower than PLA-E for CO_2 pressures up to 30 MPa. A higher plasticizing effect of PLA-I at 30 MPa and 110 °C favours an increased polymer chain mobility and their organization, which tends to a decreased free volume and lowers the sorption especially during longer exposure periods [46,58]. Unlike in the case of PLA-E, a

rise of χ_c of PLA-I from 20 to 30 MPa was evidenced, which indicates a faster crystallization of injection grade PLA in comparison to the extrusion grade PLA. An enhanced stiffness of the PLA matrix could constrain CO_2 sorption as well as thymol.

Regimes 4 and 5 were tested for the design of the SFE-SSI process, to extract thyme extract from the thyme plant and incorporate it into the PLA samples. The temperature in the extraction vessel (40 °C) was chosen in accordance with previous studies on SFE with thyme plant [33,59]. The adsorption vessel was operated at 110 °C. The results of the combined extraction and impregnation process are shown in **Table 3.**

Running the SFE-SSI with the optimal settings for d-SSI process (regimes 4 and 5) yielded thyme extract loadings around 0.4% (**Table 3**). The longer processing time had a negative effect on thyme extract loading. In opposite to pure thymol, which strongly interacts with the polymer matrix through the hydrogen bonding between the carbonyl groups of polyesters and the hydroxyl groups of thymol [60], thyme extract does not interact with the polymer matrix [46]. Accordingly, desorption of the already impregnated extract from the carrier can occur with a prolonged process time [61]. To increase the loading of thyme extract, the SFE-SSI process was performed as a semi-continuous process by stepwise re-introducing fresh CO_2 into the system every 2 h (regime 6). In contrast to regime 4, the static step was excluded to force CO_2 to flow through the plant material. The gear pump frequency was increased to 30 Hz to facilitate mass transport.

The first circulation period achieved loadings of 0.19% and 0.25% for PLA-E and PLA-I, respectively. To refill fresh CO_2, only the adsorber was depressurized to minimize extract loss [61]. It led to 3 times higher impregnations after 2 additional hours of impregnation (0.70% and 0.62% for PLA-E and PLA-I, respectively). A further step did not contribute to an increase of thyme extract load. This could be due to desorption (extraction of the extract from the carrier) after reaching the equilibrium load for the given pressure and temperature conditions as previously reported [61].

2.3. Foam morphology

All processes (s-F, s-SSI, d-SSI, SFE-SSI) produced PLA foams by depressurization of the system. The corresponding foam porosities are listed in **Table 4**. All obtained foams have micron meter-sized pores (~15 - 200 μm) (**Figs. 6-8**).

Evidently, the porosities of the PLA foams processed with s-F and s-SSI at same pressure and temperature conditions (30 MPa and 100 °C, ρ_{CO2} = 661.9 kg/m³) are similar (60 - 66%, **Table 4)**.

The SEM images are presented in **Fig. 6** and illustrate the effect of processing time and thymol loading on the morphology of the PLA-E foams. In the case of short processing time (2 h), the porosity of the foam is positively affected by the thymol loading (**Table 4**). The images with impregnated thymol (**Fig. 6b**) show larger, but still micron meter-sized (~100 - 200 μm), and evenly distributed pores with thinner lamellae than of the neat foams at the same operating conditions (**Fig. 6a**).

Figure 6

This could be due to the plasticizing effect of thymol on PLA [56,62], which leads to a reduced viscosity of the melted PLA thus allowing pores to grow larger during expansion. On the contrary, the porosity of the samples processed for 24 h is similar. The foams loaded with thymol had slightly lower porosities (**Table 4**). As discussed previously, a longer lasting exposure of semi-crystalline polymers to $scCO_2$ can increase the chain mobility and their re-arrangements into more ordered structures. This phenomenon is promoted by the presence of thymol as an additional lubricant to $scCO_2$ [15]. A prolonged soaking of PLA-E in $scCO_2$ and thymol from 2 to 24 h (**Figs. 6b** and **6c**) led to a thickening of pore lamellas as well as to a porosity decrease in the case of foams obtained by the s-SSI process (**Table 4**).

The effect of the circulation time in d-SSI process on the morphology of the PLA-E foams loaded with thymol is demonstrated in **Fig. 7**. Both SEM images show uniform and connected pores next to

some larger pores with a perforated inner surface. An increased circulation time of $scCO_2$ with dissolved thymol beyond 2 h of static mixing regime resulted in porosity increase.

Figure 7

Figure 8

The bimodal structure was also observed for the PLA-E foams obtained by the SFE-SSI process (**Fig. 8**). It could be the result of a premature phase separation due to depressurization of a larger amount of CO_2 compared to the static process. This leads to phase-separated fractions, building gas pockets which result in large cells [63,64]. Large cells reduce the bulk weight, while small cells promote the mechanical strength, which could be of interest for applications in tissue engineering and insulation applications [65–67]. The greatest porosities (74 – 76%) have been evidenced for the PLA foams obtained by the SFE-SSI process containing 0.6 – 0.7% of thyme extract (**Table 4**). This is assumed to be due to partial foaming during the adsorber decompression prior to refill of fresh CO_2 into the system. After the first decompression the sample consists of a porous structure with CO_2 bubbles trapped inside the matrix. By re-pressurizing the system, CO_2 within the bubbles dissolve back into the matrix while fresh CO_2 simultaneously penetrates the matrix from the outside. This prevents a total dissolving of all CO_2 bubbles. Some of them remain and behave as nucleation cites during a following decompression step. They promote the nucleation at them. Therefore, more CO_2 is within the polymer system and more pores are created that lead to increased porosities. Porosity decrease of the PLA-E foam with thyme extract produced by SFE-SSI process with two system re-pressurizations could be due to pore collapsing.

The foaming itself could have an effect on degree of crystallinity. To confirm this assumption, the modified HP-DSC method described in section 1.2 was used to study the plasticizing and foaming effects on the crystallinity level of PLA.

2.4. Effects of sorbed CO_2 and foaming on PLA crystallinity level analysed at atmospheric and high pressure

The effect of foaming on the degree of crystallinity (χ_c) of PLA-E was studied by methods 2 and 3 as described in section 1.2, which are a simulated foaming process in the HP-DSC apparatus and the measurement of produced neat foams in s-F. The temperatures and pressures used are between 100 - 120 °C and 10 - 30 MPa, respectively (**Table S2**). The results are visualized in **Fig. 9**. The measurements are performed either at atmospheric pressure (spheres) or at the same elevated pressure (diamonds) as the foaming itself. According to the atmospheric measurements, the PLA-E samples foamed in DSC and in the high pressure view cell (s-F process) at the same pressures, both have similar χ_c values and trends. Expectedly, the high pressure measurement of both non-foamed and foamed PLA-E samples in the DSC resulted in lower χ_c values in comparison to the atmospheric pressure measurements. This results from CO_2 plasticizing effect that leads to polymer chains loosening. Therefore, less total energy in form of melt enthalpy is required to melt the polymer (**Table S2**).

Figure 9

The absolute mean percentage difference between foamed and non-foamed samples is at about 4.5% in the considered pressure range between 10 MPa and 30 MPa, and the melting enthalpy is reduced by about 20% (**Table S2**). The level of crystallinity was more affected by plasticizing effect of the $scCO_2$ than supercritical foaming itself. The crystallinity level differs absolutely between 11% and 18% in the same pressure range (differences between the DSC foams). Accordingly, the crystallinity level of the sample foamed at 30 MPa is higher compared to one foamed at 20 MPa, when measured by DSC at atmospheric pressure. This is not the case for foamed and non-foamed samples measured at elevated pressures. The crystallinity level of non-foamed samples stays almost constant with a slight increase at 50 MPa (**Table S1**). This knowledge is of great importance wherever this material

is used, at low or high CO_2 pressures. On the other side, the crystallinity level of the polymer is changed by gas sorption in polymer matrix at the given pressure.

3. Conclusion

The present study reports on comprehensive analyses of sorbed $scCO_2$ and supercritical foaming effects on melting and crystallization behaviour of the commercial PLA for extrusion and injection moulding. An HP-DSC apparatus was used to analyse the plasticizing effect of sorbed $scCO_2$ under an extended pressure range, 10 to 50 MPa. The knowledge of the thermal behaviour was successfully employed to design and optimize batch and semi-continuous processes to incorporate natural antibacterial substances (thymol and thyme extract) into PLA and to foam it. Pressures of 20 - 30 MPa and temperatures of 100 - 120 °C were used for batch foaming and impregnation of the samples with pure thymol. The optimal conditions were identified at 30 MPa and 100 °C regarding thymol loading (4.7 - 8.5%) and foam porosity (~ 60 - 65%). Batch impregnation of PLA with thymol and semi-continuous impregnation of PLA with thyme extract, both including supercritical fluid circulation, were performed at adopted optimal conditions to optimize the processing time and the circulation regime regarding loading and foam morphology. A load of 0.71 - 1.1% of thymol and 0.6 – 0.7% of thyme extract was achieved. The semi-continuous process of SFE-SSI, which involved a partial depressurization of the system and refilling of fresh CO_2, yielded the most porous foams of around 75% porosity. The HP-DSC was used to simulate foaming and monitor the heat flow in one step. The aforementioned measurements showed a more pronounced effect of the sorbed $scCO_2$ than the supercritical foaming as well as their synergetic effect on decrease of PLA crystallinity level. The PLA foams obtained in this study can have great potential in food packaging, biomedical and insulation applications considering its porosity, biocompatibility and/or potential antibacterial and antioxidant activity.

Acknowledgements

This research project was financially supported by the project FKZ 01PL11082B, funded by a common initiative of the German Federal Government and the individual states of Germany, Serbian Ministry of Education, Science and Technological Development (Project No. III45017) and the German Academic Exchange Service (Project ID: 57140416).

References

[1] M. Nofar, C.B. Park, Poly (lactic acid) foaming, Prog. Polym. Sci. 39 (2014) 1721–1741.

[2] L.-T. Lim, R. Auras, M. Rubino, Processing technologies for poly(lactic acid), Prog. Polym. Sci. 33 (2008) 820–852.

[3] M. Chauvet, M. Sauceau, F. Baillon, J. Fages, Mastering the structure of PLA foams made with extrusion assisted by supercritical CO2, J. Appl. Polym. Sci. 134 (2017) 45067.

[4] M. Chauvet, M. Sauceau, J. Fages, Extrusion assisted by supercritical CO2: A review on its application to biopolymers, J. Supercrit. Fluids. 120 (2017) 408–420.

[5] A. Ameli, D. Jahani, M. Nofar, P.U. Jung, C.B. Park, Processing and characterization of solid and foamed injection-molded polylactide with talc, J. Cell. Plast. 49 (2013) 1–24.

[6] M. Nofar, A. Tabatabaei, A. Ameli, C.B. Park, Comparison of melting and crystallization behaviors of polylactide under high-pressure CO2, N2, and He, Polymer (Guildf). 54 (2013) 6471–6478.

[7] M. Nofar, A. Ameli, C.B. Park, The thermal behavior of polylactide with different d-lactide content in the presence of dissolved CO2, Macromol. Mater. Eng. 299 (2014) 1232–1239.

[8] M. Nofar, W. Zhu, C.B. Park, Effect of dissolved CO2 on the crystallization behavior of linear and branched PLA, Polym. (United Kingdom). 53 (2012) 3341–3353.

[9] L. Yu, H. Liu, K. Dean, L. Chen, Cold Crystallization and Postmelting Crystallization of PLA Plasticized by Compressed Carbon Dioxide, J. Polym. Sci. Part B Polym. Phys. 46 (2008)

2630–2636.

[10] L. Yu, H. Liu, K. Dean, Thermal behaviour of poly(lactic acid) in contact with compressed carbon dioxide, Polym. Int. 58 (2009) 368–372.

[11] D. Li, T. Liu, L. Zhao, X. Lian, W. Yuan, Foaming of Poly(lactic acid) Based on Its Nonisothermal Crystallization Behavior under Compressed Carbon Dioxide, Ind. Eng. Chem. Res. 50 (2011) 1997–2007.

[12] M. Mihai, M.A. Huneault, B.D. Favis, Rheology and Extrusion Foaming of Chain-Branched Poly(lactic acid), Polym. Eng. Sci. 50 (2010) 629–642.

[13] J. Reignier, J. Tatibouet, R. Gendron, Effect of Dissolved Carbon Dioxide on the Glass Transition and Crystallization of Poly(lactic acid) as Probed by Ultrasonic Measurements, Polym. Polym. Compos. 112 (2009) 1345–1355.

[14] S.C. Frerich, Biopolymer foaming with supercritical CO2-Thermodynamics, foaming behaviour and mechanical characteristics, J. Supercrit. Fluids. 96 (2015) 349–358.

[15] J. Ivanovic, S. Knauer, A. Fanovich, S. Milovanovic, M. Stamenic, P. Jaeger, et al., Supercritical CO2 sorption kinetics and thymol impregnation of PCL and PCL-HA, J. Supercrit. Fluids. 107 (2016) 486–498.

[16] E. Kiran, Supercritical fluids and polymers - The year in review - 2014, J. Supercrit. Fluids. 110 (2016) 126–153.

[17] E. Di Maio, E. Kiran, Foaming of polymers with supercritical fluids and perspectives on the current knowledge gaps and challenges, J. Supercrit. Fluids. 134 (2018) 157–166.

[18] M. Sauceau, J. Fages, A. Common, C. Nikitine, E. Rodier, New challenges in polymer foaming: A review of extrusion processes assisted by supercritical carbon dioxide, Prog. Polym. Sci. 36 (2011) 749–766.

[19] I. Tsivintzelis, G. Sanxaridou, E. Pavlidou, C. Panayiotou, Foaming of polymers with supercritical fluids: A thermodynamic investigation, J. Supercrit. Fluids. 110 (2016) 240–250.

[20] Z. Lian, S.A. Epstein, C.W. Blenk, A.D. Shine, Carbon dioxide-induced melting point depression of biodegradable semicrystalline polymers, J. Supercrit. Fluids. 39 (2006) 107–117.

[21] S. Takahashi, J.C. Hassler, E. Kiran, Melting behavior of biodegradable polyesters in carbon dioxide at high pressures, J. Supercrit. Fluids. 72 (2012) 278–287.

[22] E. Huang, X. Liao, C. Zhao, C.B. Park, Q. Yang, G. Li, Effect of Unexpected CO2's Phase Transition on the High-Pressure Differential Scanning Calorimetry Performance of Various Polymers, ACS Sustain. Chem. Eng. 4 (2016) 1810–1818.

[23] Z. Zhang, Y.P. Handa, High-pressure calorimetric study of plasticization of poly(methyl methacrylate) by methane, ethylene, and carbon dioxide, J. Polym. Sci. Part B Polym. Phys. 36 (1998) 977–982.

[24] M. Takada, S. Hasegawa, M. Ohshima, Crystallization Kinetics of Poly(L-lactide) in Contact With Pressurized CO2, Polym. Eng. Sci. 44 (2004) 186–196.

[25] W. Ding, T. Kuboki, A. Wong, C.B. Park, M.M. Sain, B. Park, et al., Rheology, thermal properties, and foaming behavior of high D-content polylactic acid/ cellulose nanofiber composites, RSC Adv. 5 (2015) 91544–91557.

[26] D. Westerman, S. Nalawade, Analysis of melting point depression in biodegradable polymers using supercritical carbon dioxide by golden gate IR and high pressure DSC, in: Proc. 11th Eur. Meet. Supercrit. Fluids, Barselona, 2008. http://www.isasf.net/fileadmin/files/Docs/Barcelona/ISASF 2008/PDF/Oral communications/OC_TT_1.pdf (accessed November 6, 2014).

[27] M.A. Fanovich, J. Ivanovic, P.T. Jaeger, An Integrated Supercritical Extraction and Impregnation Process for Production of Antibacterial Scaffolds, in: C. Domingo, P. Subra (Eds.), Supercrit. Fluid Nanotechnol. Adv. Appl. Compos. Hybrid Nanomater., Pan Stanford Publishing Pte Ltd, Boca Raton, FL, 2016: pp. 297–323.

[28] Z. Zhang, Y.P. Handa, CO2-Assisted Melting of Semicrystalline Polymers†, Macromolecules. 30 (1997) 8505–8507.

[29] E. Aionicesei, M. Škerget, Ž. Knez, Measurement of CO2 solubility and diffusivity in poly(L-lactide) and poly(D,L-lactide-co-glycolide) by magnetic suspension balance, J. Supercrit. Fluids. 47 (2008) 296–301.

[30] M.A. Fanovich, J. Ivanovic, I. Zizovic, D. Misic, P. Jaeger, Functionalization of polycaprolactone/hydroxyapatite scaffolds with Usnea lethariiformis extract by using supercritical CO2, Mater. Sci. Eng. C. 58 (2016) 204–212.

[31] M.A. Fanovich, J. Ivanovic, D. Misic, M.V. Alvarez, P. Jaeger, I. Zizovic, et al., Development of polycaprolactone scaffold with antibacterial activity by an integrated supercritical extraction and impregnation process, J. Supercrit. Fluids. 78 (2013) 42–53.

[32] S. Milovanovic, D. Markovic, K. Aksentijevic, D.B. Stojanovic, J. Ivanovic, I. Zizovic, Application of cellulose acetate for controlled release of thymol, Carbohydr. Polym. 147 (2016) 344–353.

[33] J. Ivanovic, D. Misic, I. Zizovic, M. Ristic, In vitro control of multiplication of some food-associated bacteria by thyme, rosemary and sage isolates, Food Control. 25 (2012) 110–116.

[34] A.C. de Souza, A.M.A. Dias, H.C. Sousa, C.C. Tadini, Impregnation of cinnamaldehyde into cassava starch biocomposite films using supercritical fluid technology for the development of food active packaging, Carbohydr. Polym. 102 (2014) 830–837.

[35] M.A. Del Nobile, A. Conte, A.L. Incoronato, O. Panza, Antimicrobial efficacy and release kinetics of thymol from zein films, J. Food Eng. 89 (2008) 57–63.

[36] A. Torres, J. Romero, A. Macan, A. Guarda, M.J. Galotto, Near critical and supercritical impregnation and kinetic release of thymol in LLDPE films used for food packaging, J. Supercrit. Fluids. 85 (2014) 41–48.

[37] A. Wattanasatcha, S. Rengpipat, S. Wanichwecharungruang, Thymol nanospheres as an

effective anti-bacterial agent, Int. J. Pharm. 434 (2012) 360–365.

[38] S. Cosentino, C.I. Tuberoso, B. Pisano, M. Satta, V. Mascia, E. Arzedi, et al., In-vitro antimicrobial activity and chemical composition of Sardinian Thymus essential oils, Lett. Appl. Microbiol. 29 (1999) 130–135.

[39] A. Nostro, A.R. Blanco, M.A. Cannatelli, V. Enea, G. Flamini, I. Morelli, et al., Susceptibility of methicillin-resistant staphylococci to oregano essential oil, carvacrol and thymol, FEMS Microbiol. Lett. 230 (2004) 191–195.

[40] S. Milovanovic, M. Stamenic, D. Markovic, M. Radetic, I. Zizovic, Solubility of thymol in supercritical carbon dioxide and its impregnation on cotton gauze, J. Supercrit. Fluids. 84 (2013) 173–181.

[41] A. Torres, E. Ilabaca, A. Rojas, F. Rodríguez, M.J. Galotto, A. Guarda, et al., Effect of processing conditions on the physical, chemical and transport properties of polylactic acid films containing thymol incorporated by supercritical impregnation, Eur. Polym. J. 89 (2017) 195–210.

[42] I. Kikic, F. Vecchione, Supercritical impregnation of polymers, Curr. Opin. Solid State Mater. Sci. 7 (2003) 399–405.

[43] Y.T. Shieh, J.H. Su, G. Manivannan, P.H.C. Lee, S.P. Sawan, W.D. Spall, Interaction of supercritical carbon dioxide with polymers. I. Crystalline polymers, J. Appl. Polym. Sci. 59 (1996) 695–705.

[44] T. Fujiwara, T. Yamaoka, Y. Kimura, K.J. Wynne, Poly(lactide) swelling and melting behavior in supercritical carbon dioxide and post-venting porous material, Biomacromolecules. 6 (2005) 2370–2373.

[45] E. Aionicesei, M. Škerget, Ž. Knez, Solubility and Diffusivity of Supercritical CO2 in Bioresorbable Polymers : Measurements, Calculations and Potential Applications in Polymer Foaming, in: 12th Eur. Meet. Supercrit. Fluids, ISASF, International Society for Advancement

of Supercritical Fluids, Graz, 2010: pp. 1–10.

[46] S. Milovanovic, G. Hollermann, C. Errenst, J. Pajnik, S. Frerich, S. Kroll, et al., Supercritical CO2 impregnation of PLA/PCL films with natural substances for bacterial growth control in food packaging, Food Res. Int. 107 (2018) 486–495.

[47] M. Champeau, J.-M. Thomassin, T. Tassaing, C. Jérôme, Drug loading of sutures by supercritical CO2 impregnation: effect of polymer/drug interactions and thermal transitions, Macromol. Mater. Eng. 300 (2015) 596–610.

[48] M. Nofar, A. Ameli, C.B. Park, Development of polylactide bead foams with double crystal melting peaks, Polymer (Guildf). 69 (2015) 83–94.

[49] W.Y. Jang, B.Y. Shin, T.J. Lee, R. Narayan, Thermal Properties and Morphology of Biodegradable PLA / Starch Compatibilized Blends, J. Ind. Eng. Chem. 13 (2007) 457–464.

[50] R.C. Roberts, The melting behavior of bulk crystallized polymers, J. Polym. Sci. Part B Polym. Lett. 8 (1970) 381–384.

[51] T. Yokohara, M. Yamaguchi, Structure and properties for biomass-based polyester blends of PLA and PBS, Eur. Polym. J. 44 (2008) 677–685. doi:10.1016/j.eurpolymj.2008.01.008.

[52] O. Martin, L. Avérous, Poly(lactic acid): Plasticization and properties of biodegradable multiphase systems, Polymer (Guildf). 42 (2001) 6209–6219.

[53] L. Cartier, T. Okihara, Y. Ikada, H. Tsuji, J. Puiggali, B. Lotz, et al., Epitaxial crystallization and crystalline polymorphism of polylactides, Polymer (Guildf). 41 (2000) 8909–8919.

[54] M.L. Di Lorenzo, R. Androsch, Melting of α′- and α-crystals of poly(lactic acid), AIP Conf. Proc. 1736 (2016) 020009.

[55] M.K. Trivedi, S. Patil, R.K. Mishra, S. Jana, Structural and Physical Properties of Biofield Treated Thymol and Menthol, J. Mol. Pharm. Org. Process Res. 3 (2015) 1000127. doi:10.4172/2329-9053.1000127.

[56] S. Milovanovic, M. Stamenic, D. Markovic, J. Ivanovic, I. Zizovic, Supercritical

impregnation of cellulose acetate with thymol, J. Supercrit. Fluids. 97 (2015) 107–115.

[57] R. Span, W. Wagner, A new equation of state for carbon dioxide covering the fluid region from the triple-point temperature to 1100 K at pressures up to 800 MPa, J. Phys, Chem. Ref. Data. 25 (1996) 1509–1596.

[58] M.R. Mauricio, F.C.G. Manso, M.H. Kunita, D.S. Velasco, A.C. Bento, E.C. Muniz, et al., Synthesis and characterization of ZnO/PET composite using supercritical carbon dioxide impregnation technology, Compos. Part A Appl. Sci. Manuf. 42 (2011) 757–761.

[59] J. Ivanovic, I. Zizovic, M.M. Ristic, M. Stamenic, D. Skala, The analysis of simultaneous clove/oregano and clove/thyme supercritical extraction, J. Supercrit. Fluids. 55 (2011) 983–991.

[60] K. Boonruang, W. Chinsirikul, B. Hararak, N. Kerddonfag, V. Chonhenchob, Antifungal Poly(lactic acid) Films Containing Thymol and Carvone, MATEC Web Conf. 67 (2016) 06107.

[61] J. Ivanovic, S. Milovanovic, M. Stamenic, M.A. Fanovich, P. Jaeger, I. Zizovic, Application of an Integrated Supercritical Extraction and Impregnation Process for Incorporation of Thyme Extracts into Different Carriers, in: J. Osborne (Ed.), Handb. Supercrit. Fluids Fundam. Prop. Appl., Nova Science Publishers, Inc., Hauppauge, N.Y. USA, 2014: pp. 257–280.

[62] M. Ramos, E. Fortunati, M. Peltzer, F. Dominici, A. Jiménez, M. del C. Garrigós, et al., Influence of thymol and silver nanoparticles on the degradation of poly(lactic acid) based nanocomposites: Thermal and morphological properties, Polym. Degrad. Stab. 108 (2014) 158–165.

[63] M. Mihai, M.A. Huneault, B.D. Favis, Crystallinity Development in Cellular Poly(lactic acid) in the Presence of Supercritical Carbon Dioxide, J. OfAppliedPolymer Sci. 113 (2009) 2920–2932.

[64] A. Salerno, E. Di Maio, S. Iannace, P.A. Netti, Solid-state supercritical CO2 foaming of PCL and PCL-HA nano-composite: Effect of composition, thermal history and foaming process on foam pore structure, J. Supercrit. Fluids. 58 (2011) 158–167.

[65] P. Yu, H.-Y. Mi, A. Huang, L.-H. Geng, B.-Y. Chen, T.-R. Kuang, et al., Effect of Poly(butylenes succinate) on Poly(lactic acid) Foaming Behavior: Formation of Open Cell Structure, Ind. Eng. Chem. Res. 54 (2015) 6199–6207.

[66] S.G. Mosanenzadeh, H.E. Naguib, C.B. Park, N. Atalla, Development of polylactide open-cell foams with bimodal structure for high-acoustic absorption, J. Appl. Polym. Sci. 131 (2014) 1–11.

[67] K.-M. Lee, E.K. Lee, S.G. KIM, C.B. Park, H.E. Naguib, Bi-cellular Foam Structure of Polystyrene from Extrusion Foaming Process, J. Cell. Plast. 45 (2009) 539–553.

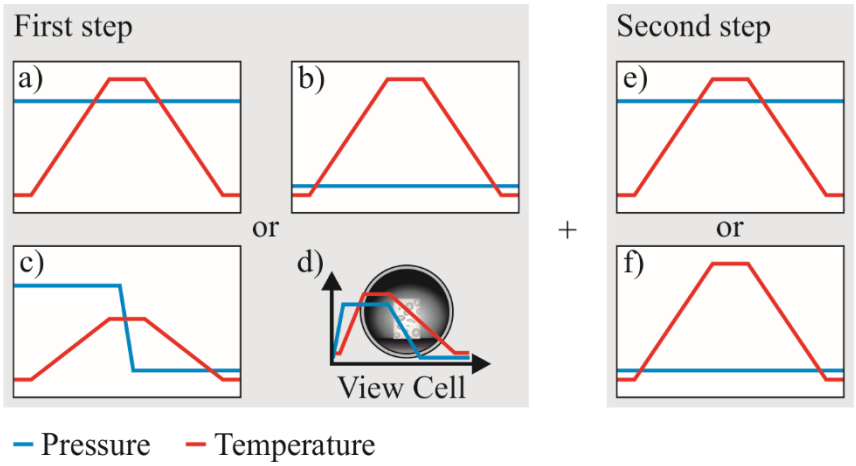

Fig. 1. Various pressure and temperature profiles of HP-DSC measurements: a) – d) represent pre-treatments of pure or foamed samples: Thermal pre-treatment of PLA at a) high and b) atmospheric pressure; c) Foaming profile; d) Batch foaming in view cell. e) – f) are measure profiles at e) high and f) atmospheric pressure.

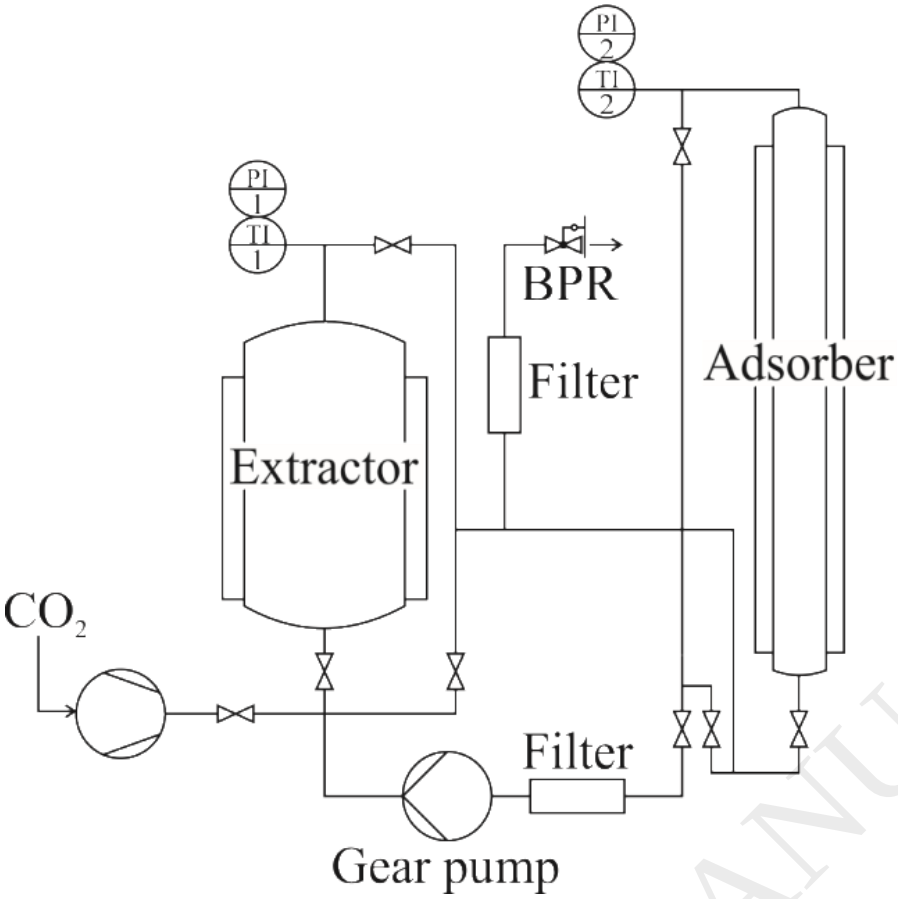

Fig. 2. A schematic presentation of the HPEA unit for the d-SSI and SFE-SSI processes.

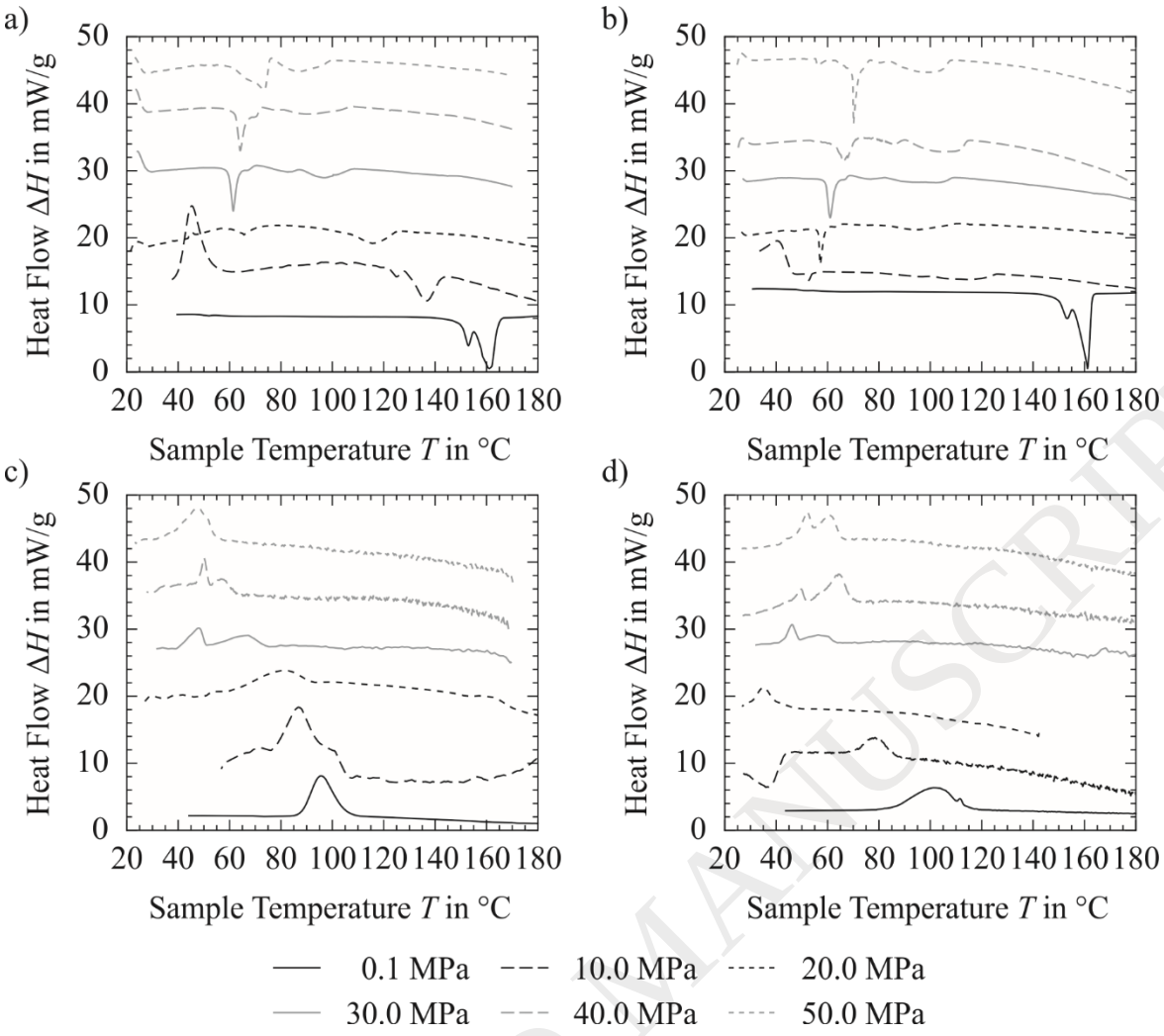

Fig. 3. Heating thermograms of a) PLA-E and b) PLA-I and cooling thermograms of c) PLA-E and d) PLA-I at atmospheric pressure and 10- 50 MPa of CO_2 pressure.

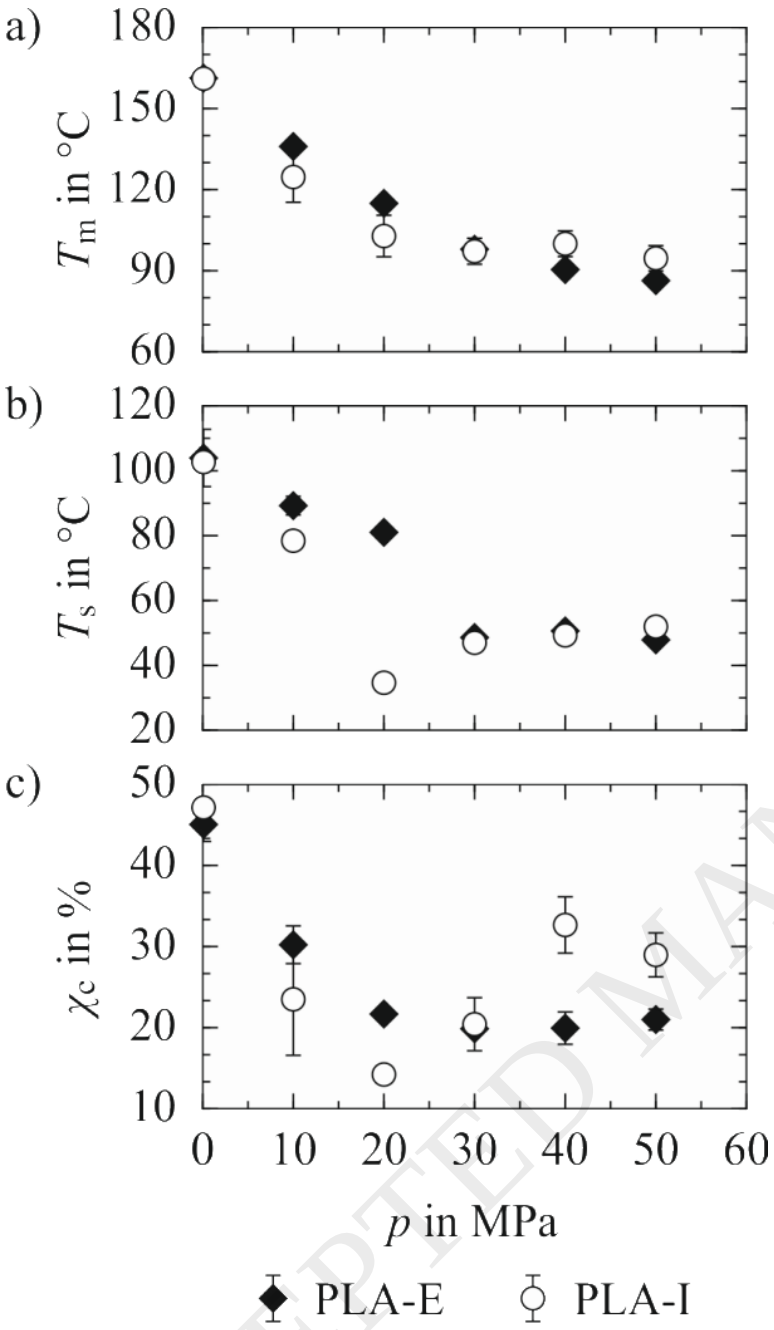

Fig. 4. a) The melting temperature (T_m), b) the crystallization temperature (T_s) and c) the degree of crystallinity (χ_c) of PLA-E and PLA-I at different CO_2 pressures.

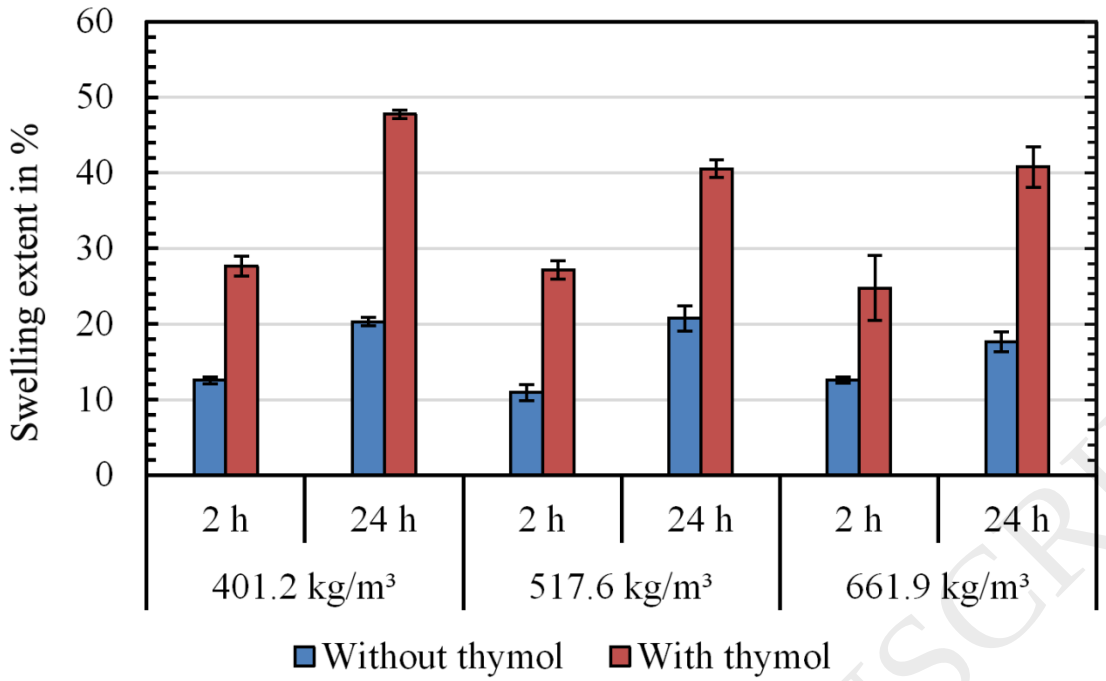

Fig. 5. The effect of sorbed $scCO_2$ and thymol on the PLA-E swelling.

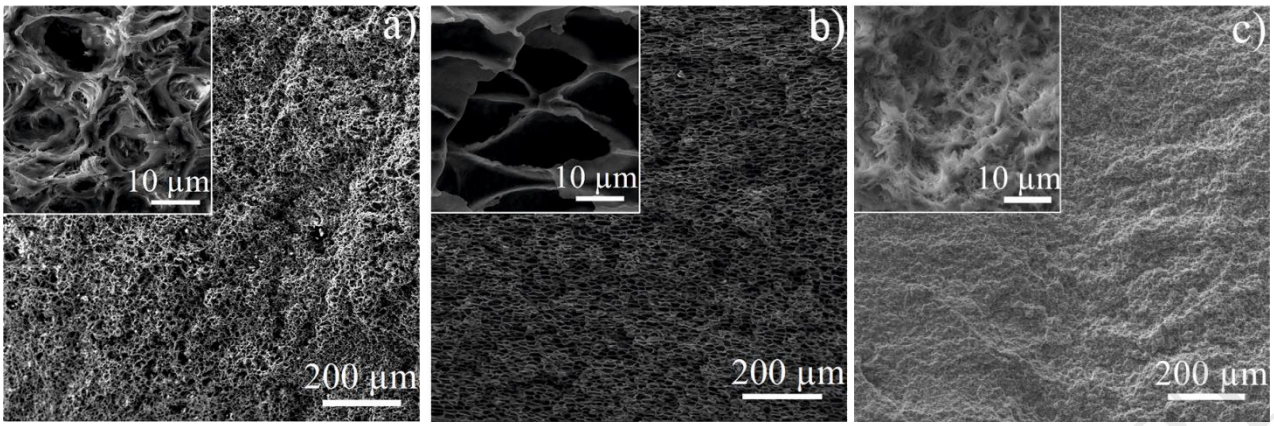

Fig. 6. SEM images of PLA-E foams processed at 30 MPa and 100 °C by a) 2 h s-F, b) 2 h s-SSI with thymol and c) 24 h s-SSI with thymol.

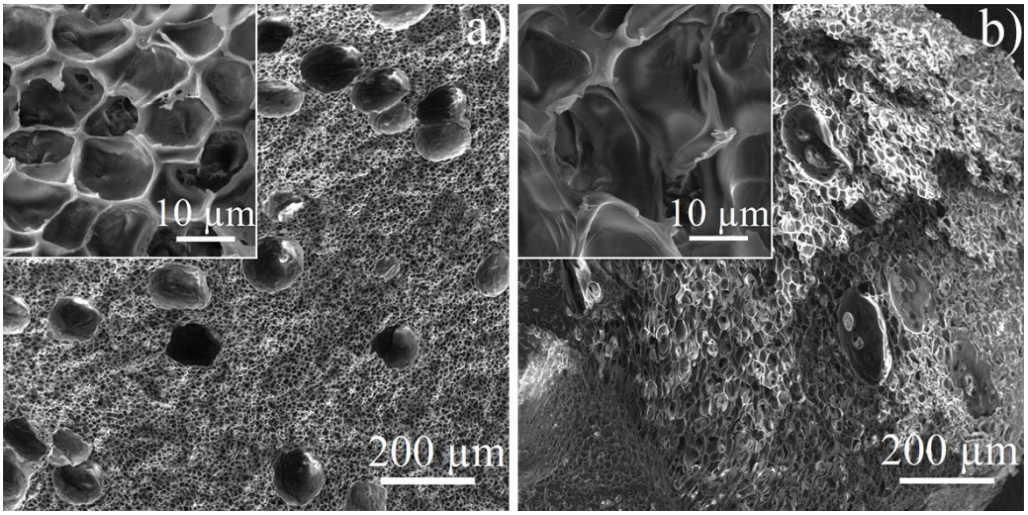

Fig. 7. SEM images of PLA-E foams impregnated with thymol by d-SSI process after 2 h of static and a) 2 h (regime 4) or b) 5 h of dynamic impregnation (regime 5).

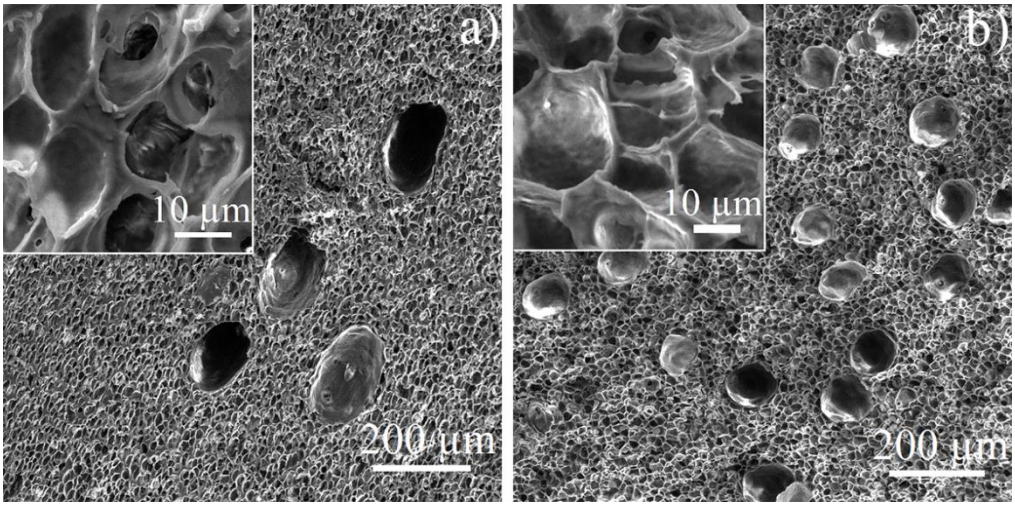

Fig. 8. SEM images of PLA-E foams impregnated with thyme extract produced by SFE-SSI process using regime 6 with a) 2 + 2 h and b) 2 + 2 + 2 h of dynamic mixing regime.

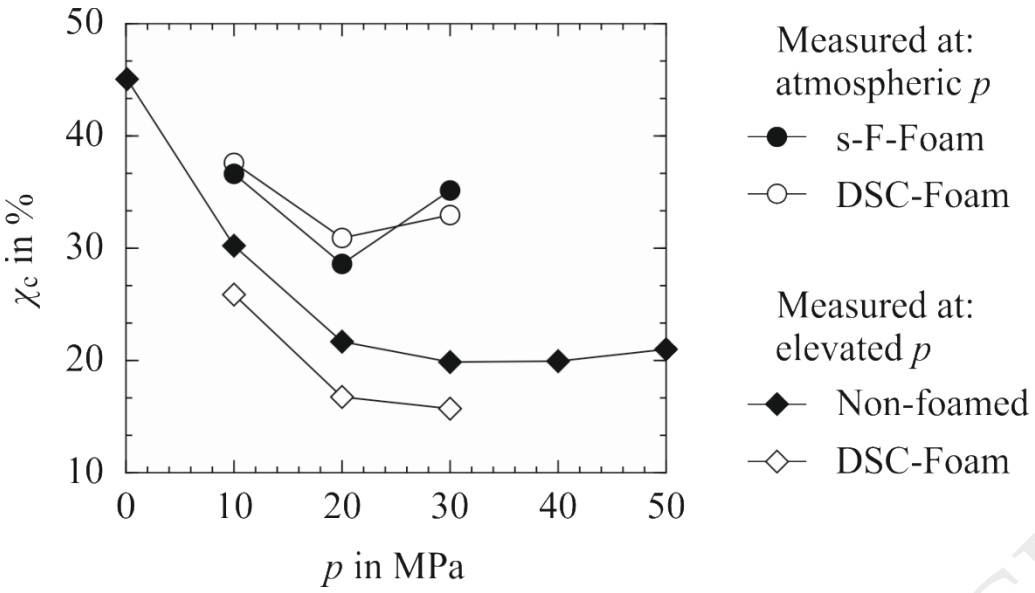

Fig. 9. Effects of sorbed CO_2 and supercritical foaming on crystallinity level of PLA-E.

Table 1

Thymol loading in PLA-E achieved after 2 h and 24 h in s-SSI.

p	***T***	ρ_{CO2} [a]	***t***	***L***
MPa	°C	kg/m³	h	%
20	120	401.2	2	11.0 ± 1.2
			24	19.8 ± 0.8
24	112	517.6	2	7.9 ± 0.4
			24	11.4 ± 0.7
30	100	661.9	2	4.7 ± 0.4
			7	5.6 ± 0.4
			24	8.5 ± 1.6

[a] Calculated using Span and Wagner EOS [57]

Table 2

Achieved thymol loadings in the PLA samples by d-SSI process.

Sample	**Regime**	t_{st}	t_{dyn}	**Gear pump frequency**	***L***
	#	h	h	Hz	%
PLA-E	1	0	2	30	0.36 ± 0.05
	2	0	2	10	0.41 ± 0.06
	3	0	4	10	0.38 ± 0.06
	4	2	2	10	0.71 ± 0.11
	5	2	5	10	1.10 ± 0.19
PLA-I	4	2	2	10	0.54 ± 0.08
	5	2	5	10	0.20 ± 0.03

Table 3

Thyme extract loading of the PLA samples processed by SFE-SSI process.

Sample	**Number of cycles**	**Regime**	m_{CO2}/m_{Thyme}	t_{st}	t_{dyn}	**Gear pump frequency**	***L***
		#	-	h	h	Hz	%
PLA-E	1	4	15.92	2	2	10	0.43 ± 0.04
	1	5	17.91	2	5	10	0.32 ± 0.03
	2	6[a]	15.91	0	2	30	0.19 ± 0.02
			25.85		2		0.70 ± 0.07
			35.75		2		0.62 ± 0.06
PLA-I	2	6[a]	15.92	0	2	30	0.25 ± 0.02
			23.88		2		0.62 ± 0.06

[a] Fresh CO_2 is introduced every 2 h.

Table 4

The foam porosities (ε) and densities (ρ_f) of the PLA-E and PLA-I samples with and without thymol (T) or thyme extract (TE).

Sample	**Process**	ρ_{CO2}	t_{st}	t_{dyn}	ρ_f	ε
		kg/m³	h	h	kg/m³	%
PLA-E	s-F	401.2	24	-	506.6 ± 16.3	54.8 ± 1.3
		517.6	24	-	427.6 ± 12.0	65.5 ± 1.0
		661.9	2	-	685.2 ± 99.6	44.6 ± 8.0
		661.9	24	-	426.0 ± 37.1	65.6 ± 3.0
PLA-I	s-F	661.9	24	-	477.7 ± 30.8	61.6 ± 2.5
PLA-E + T	s-SSI	661.9	2	-	470.7 ± 42.5	62.4 ± 3.4
		661.9	24	-	490.3 ± 5.8	60.4 ± 0.7
PLA-E + T	d-SSI	E: 909.9 A: 622.3	2	2	472.2 ± 7.0	61.9 ± 0.6
		E: 909.9 A: 622.3	2	5	433.2 ± 16.6	65.1 ± 1.3
PLA-E + TE	SFE-SSI	E: 909.9 A: 622.3	0	2 + 2	299.4 ± 20.0	75.8 ± 1.6
		E: 909.9 A: 622.3	0	2 + 2 + 2	420.6±185	64.4±15.0
PLA-I + TE	SFE-SSI	E: 909.9	0	2 + 2	320.5 ± 84.7	73.9 ± 6.8

		A: 622.3				
E: Extractor; A: Adsorber.						